SCIENTIFIC REPORTS

OPEN

# Photocatalytic Degradation of Bisphenol-A using N, Co Codoped $TiO_2$ Catalyst under Solar Light

Received: 2 May 2018
Accepted: 13 December 2018
Published online: 24 January 2019

Alok Garg[1], Tejasvi Singhania[2], Ashutosh Singh[3], Shilpa Sharma[4], Sonam Rani[2], Ananya Neogy[5], Shri Ram Yadav[5], Vikas Kumar Sangal[6] & Neha Garg[3]

**Advanced oxidation processes (AOPs) including heterogeneous photocatalysis has proven as one of the best technique for waste-water treatment. Photocatalytic process using semiconductor like $TiO_2$ based heterogeneous photocatalysis is a promising method for the treatment of toxic pollutants. In the present study, visible-light photoactive cobalt and nitrogen co-doped $TiO_2$ nanoparticles were synthesized via wet impregnation method. The photocatalysts were characterized using X-ray diffraction (XRD), Raman Spectra, Fourier Transform Infrared (FTIR) Spectroscopy, Scanning Electron Microscopy (SEM), Transmission Electron Microscope (TEM), UV-vis spectrophotometer and X-ray photoelectron spectrophotometer (XPS). The photocatalytic activitiy of prepared (N, Co)-codoped $TiO_2$ on the mineralization of Bisphenol-A (BPA) under visible light irradiation was studied and the results were compared to commercial $TiO_2$ (Degussa P25). The results demonstrated that 1.5% Co and 0.5% N – codoped $TiO_2$ samples revealed higher activity than commercial $TiO_2$. Total organic carbon (TOC) removal was observed to be 97%, which indicate the complete mineralization of BPA. GC-MS analysis was carried to find out the possible intermediates formed and reaction pathway.**

In today's world poor sanitation, waterborne infections, water quality declination, and absence of clean water supply are a great concern arose due to increase in population. The impacts of chemicals like colors, herbicides, pesticides etc. discharge in streams and lakes that are suspected to be endocrine-disrupting chemicals (EDCs) are creating havoc on the biological systems. Despite of the fact that it is still perplex for analysts whether such chemicals have an impact upon people or not, nevertheless it is important to create productive strategies for degradation of these EDCs from wastewater[1].

Bisphenol-A [2,2-bis (4-hydroxyphenyl) propane] or BPA is generally utilized as a beginning material for epoxy and polycarbonate plastics. BPA from plastic items into water has as of late been identified as a genuine reason of water contamination. Also, high concentrations of BPA can be contained in wastewater from its creation plants. BPA enters into the water bodies through generation units and by drainage made by BPA-based saps[2]. Microorganism can effectively degrade BPA but requires long time for the wastewater containing BPA. Therefore, we require the simple and cheap strategies for degradation of BPA in wastewater.

A number of physical, chemical, and biological techniques have been developed over the last two decades to remove toxicity from pharmaceutical wastewater but these treatment methods have also their disadvantages. These methods are not much efficient to bring down the pollution parameters to the satisfactory level. The current techniques for treatment relies on the development of receptive synthetic species, a method termed as advance oxidation processes (AOPs). AOPs are used for degradation of wastewater containing bio-recalcitrant organic pollutants or removal of pathogens. AOPs produced highly reactive chemical species like hydroxyl radicals that completely destroy the pollutants present in wastewater. The central point influencing the AOPs are pH, convergence of the waste to be dealt with, catalyst loading included, UV illumination and time[3].

[1]Department of Chemical Engineering, Thapar Institute of Engineering & Technology, Patiala, 147004, India. [2]School of Chemistry and Biochemistry, Thapar Institute of Engineering & Technology, Patiala, 147004, India. [3]School of Basic Sciences, Indian Institute of Technology Mandi, Mandi, 175005, India. [4]School of Science, Sandip University, Nashik, Maharashtra, 422213, India. [5]Department of Biotechnology, Indian Institute of Technology Roorkee, Roorkee, 247667, India. [6]Department of Chemical Engineering, Malaviya National Institute of Technology, Jaipur, India. Correspondence and requests for materials should be addressed to A.G. (email: alok.garg.chem@gmail.com) or N.G. (email: neha@iitmandi.ac.in)

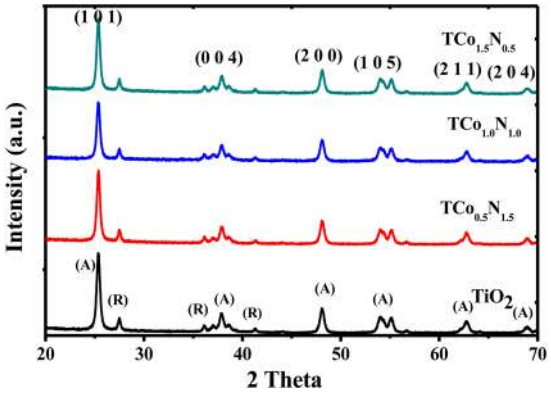


**Figure 1.** X-ray diffraction pattern of different photocatalysts.

Titanium dioxide ($TiO_2$) is one the most efficient phototocatalysts used for photocatalytic oxidation of organic pollutants present in wastewater[4]. Under UV irradiation, $TiO_2$ is photo activated and active oxygen species such as hydroxyl radicals are formed on the surfaces of the $TiO_2$ crystals. Most of the organic compounds could be decomposed into $CO_2$ and $H_2O$ by the attack of these radicals that possess high oxidizing power. $TiO_2$ photocatalysis in aqueous medium yields a variety of intermediates. It is chemically and photochemically stable, but is only excited by ultraviolet light having wavelength ($\lambda$) less than 390 nm, therefore the light utilization efficiency to solar irradiation and a fluorescent lamp is quite low. To conquer the portion of the troubles experienced, diverse dopants are being explored with the point of upgrading the morphology of $TiO_2$ in the photocatalysis. Dopants adjust the electronic structure of $TiO_2$ to widen its viable scope of light affectability for photocatalysis from the ultra-violet (UV) area to the distinctive light locale. Therefore, attempts were made to extend the absorption range of titanium dioxide into the visible-light region by the introduction of a donor level by transition metal doping. The main aim of these activities includes the (i) combination of energy levels into the band gap of $TiO_2$, (ii) changing the life time of photogenerated charge carriers, (iii) swap of the $Ti^{4+}$ with cation of the identical size, and (iv) shifting the VB and/or the CB in order to enable the process of photo-excitation at lesser energies, achievement of which depends on the method of preparation[5–7]. In order to alter the optical response of $TiO_2$ photocatalysts, doping and codoping of titania is an effective method to alter the band gap energy. The main objective of doping is to decrease the band gap of $TiO_2$, i.e., to induce a bathochromic shift and thus to extend its wavelength range response to the visible region[8].

Various studies have been devoted to achieve desired band gap narrowing of titania by using non-metals such as nitrogen (N), phosphorous (P), sulfur (S), fluorine (F), and carbon (C)[9–15]. Nitrogen has been reported to be the most promising dopant as it can easily substitute oxygen (O) in the $TiO_2$ lattice owing to its atomic size comparable with that of O, small ionization energy and high stability. Non-metal dopants P and S have also been reported to show optimistic outcomes for visible light activity in titania photocatalysts[4,16]. For the non-metal-doped titania photocatalysts, the mixing of N, S or C (2p) O (2p) states shifts the VB edge upwards, resulting in a decrease of the band gap of the N-doped $TiO_2$ and thereby the photocatalyst can be energetic under visible light irradiation. The doping of a range of transition metal ions in to $TiO_2$ could shift its optical absorption edge from UV to visible light range[17]. At a high dopant concentration, the metal ions can behave as recombination centers for the photoinduced charge carriers thereby, decreasing the quantum efficiency[16,18]. Vanadium[17,19], copper[20,21] and cobalt[22] doping on $TiO_2$ offers a possible promising strategy to enhance the characteristics of photocatalytic species and activity under visible light.

In an effort to study the effect of surface co-modifications on photocatalytic degradation and characteristic aspects of photo-induced charge properties and possible synergic effects between the introduced components, the proposed study was undertaken with following objectives: (i) to synthesize the Co, N codoped $TiO_2$, (ii) characterization of synthesized codoped $TiO_2$, and (iii) photocatalytic activity (Degradation of BPA) of Co, N codoped $TiO_2$ under solar light.

## Results and Discussion

**Characterization of photocatalysts.** *X-ray diffraction (XRD).* The XRD patterns of N, Co codoped $TiO_2$ catalyst indicates that the structure consists of anatase and rutile phases while undoped $TiO_2$ exhibits the pure anatase phase as shown in Fig. 1. XRD peaks (1 0 1), (0 0 4), (2 0 0), (1 0 5), (2 1 1) and (2 0 4) were identified corresponding to anatase phase (ICDD No. 86–1048, 86–1157) and 2Theta = 27.4° corresponds to the rutile phase for codoped $TiO_2$ photocatalyst[23]. The anatase and rutile phase contents of the codoped $TiO_2$ were calculated by analyzing the intensities of anatase 101 peak at 2θ = 25.5° and rutile 110 peak at 2θ = 27.5°. The anatase % (A%) was found by the following equation:

$$Percentage\ of\ Anatase\ (\%A) = \frac{100}{1 + 1.265\frac{I_R}{I_A}} \quad (1)$$

| Catalyst sample | 2 Theta (degree) (101) | d-spacing (Å) | Anatase lattice parameters (Å) | | Phase | | Energy band gap (eV) | Wavelength (nm) |
|---|---|---|---|---|---|---|---|---|
| | | | a = b | C | % A | % R | | |
| T | 25.377 | 3.5140 | 3.7822 | 9.5023 | 66.78 | 33.22 | 3.2 | 387 |
| $TCo_{0.5}N_{1.5}$ | 25.325 | 3.5140 | 3.7822 | 9.5023 | 70.47 | 29.53 | 2.88 | 430 |
| $TCo_{1.0}N_{1.0}$ | 25.308 | 3.5162 | 3.7842 | 9.5146 | 64.68 | 35.32 | 3.10 | 400 |
| $TCo_{1.5}N_{0.5}$ | 25.325 | 3.5140 | 3.7822 | 9.5023 | 74.25 | 25.75 | 2.85 | 435 |

**Table 1.** Physicochemical properties and calculated energy band gap of codoped $TiO_2$ samples.

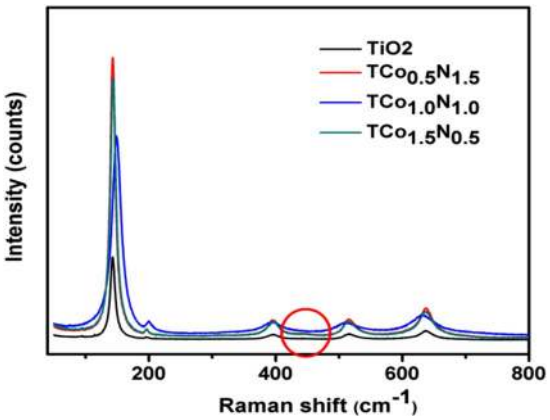


**Figure 2.** Raman spectra of $TiO_2$ and its formulation.

$$Percentage\ of\ Rutile\ (\%R) = 100 - \%A \tag{2}$$

where $I_A$ is the intensity of the 101 peak of anatase and $I_R$ is the intensity of the 110 peak of rutile. From equations 2 and 3, anatase phase has been found to be 74.25% and rutile phase was 25.75% in the N, Co codoped $TiO_2$ (Table 1). The average crystallite size of the sample has been estimated using Debye-Scherer equation:

$$d = \frac{0.89\lambda}{\beta \cos\theta} \tag{3}$$

where d represents the crystallite size, λ is the wave length of incident X-ray, β is the full width at half maximum, and θ represents the scattering angle. The mean grain size of the N, Co codoped $TiO_2$ has been estimated as 3.5 nm by Debye-Scherer's equation (Table 1).

*Raman Spectroscopy.* Raman spectroscopy provides the important data for the presence of different phases in $TiO_2$. The anatase phase of undoped. $TiO_2$ has six Raman active modes in the vibrational spectrum centered around 144 $cm^{-1}$, 197 $cm^{-1}$, 399 $cm^{-1}$, 513 $cm^{-1}$, 519 $cm^{-1}$, and 639 $cm^{-1}$ corresponding to $E_g$, $E_g$, $B_{1g}$, $A_{1g}$, $B_{1g}$ and $E_g$ respectively[24] whereas the rutile $TiO_2$ shows four Raman-active fundamental modes at around 143 $cm^{-1}$, 447 $cm^{-1}$, 612 $cm^{-1}$ and 826 $cm^{-1}$ corresponding to $B_{1g}$, $E_g$, $A_{1g}$, and $B_{2g}$ respectively for first-order effect[25]. In the present study, the Raman spectra measured confirmed the anatase phase for undoped $TiO_2$ and gives the bands at 143 $cm^{-1}$ ($E_g$), 197 $cm^{-1}$ ($E_g$), 399 $cm^{-1}$ ($B_{1g}$), 517 $cm^{-1}$ ($A_{1g} + B_{1g}$), and 639 $cm^{-1}$ ($E_g$) whereas the doped $TiO_2$ gives similar bands as of undoped $TiO_2$ with an additional small band at 447 $cm^{-1}$ ($E_g$) confirming the presence of anatase and rutile phase in the codoped $TiO_2$ (Fig. 2). As seen from Fig. 2, the signature peak of $TiO_2$ in the codoped sample is significantly shifted, compared to that of the commercial $TiO_2$ sample, which may be ascribed to the reduction in crystallite sizes in the codoped $TiO_2$[26]. The reduction in the size of the particles also been confirmed by the help of SEM data. The obtained results from the Raman spectra are in perfect agreement with the literature reports and also corroborate well with the powder XRD and TEM results.

*Fourier transform infrared (FTIR) spectroscopy.* FTIR patterns of the doped and codoped $TiO_2$ particles were taken to get the information on the surface chemistry of the particles as shown in Fig. 3. The bands were observed in the range of 3670–3000 $cm^{-1}$ and 1576–1710 $cm^{-1}$ in undoped and all codoped $TiO_2$ particles and were attributed to -OH stretching vibration and -OH bending respectively. Additionally, a band in the fingerprint region around 560–760 $cm^{-1}$ in all the samples was attributed to the Ti-O-Ti stretching vibration[27]. FTIR pattern did not exhibit any band equivalent to the doped or co-doped metal oxide due to their low weight percentage.

*Scanning Electron Microscopy (SEM).* Figure 4 shows typical SEM micrographs of $TiO_2$, and codoped $TiO_2$. A detailed SEM investigation of the particle surfaces states that the primary particles are quite uniform in size and roughly spherical in shape, and that the agglomerates are fused together to form relatively larger uneven grains.

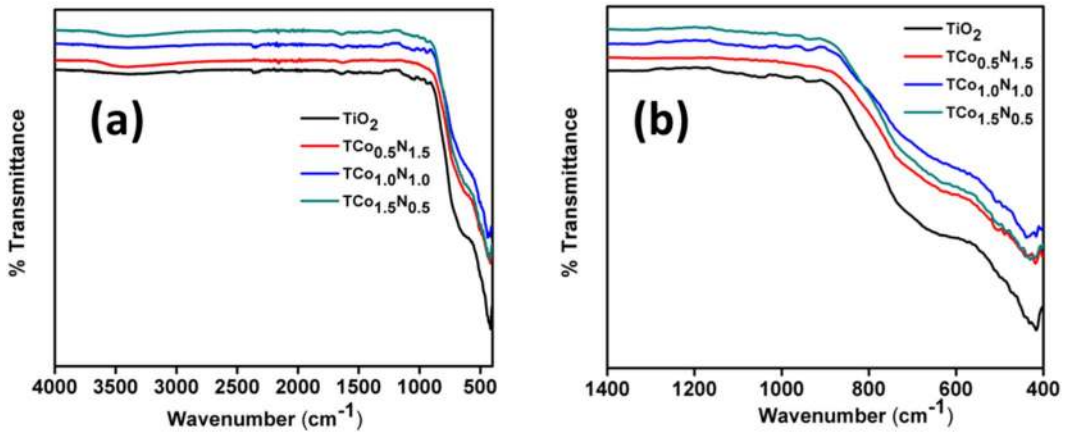


**Figure 3.** FTIR spectra (**a**) whole, and (**b**) figure print region of (**a**) $TiO_2$, (**b**) $TCo_{0.5}N_{1.5}$, (**c**) $TCo_{1.0}N_{1.0}$ and (**d**) $TCo_{1.5}N_{0.5}$.

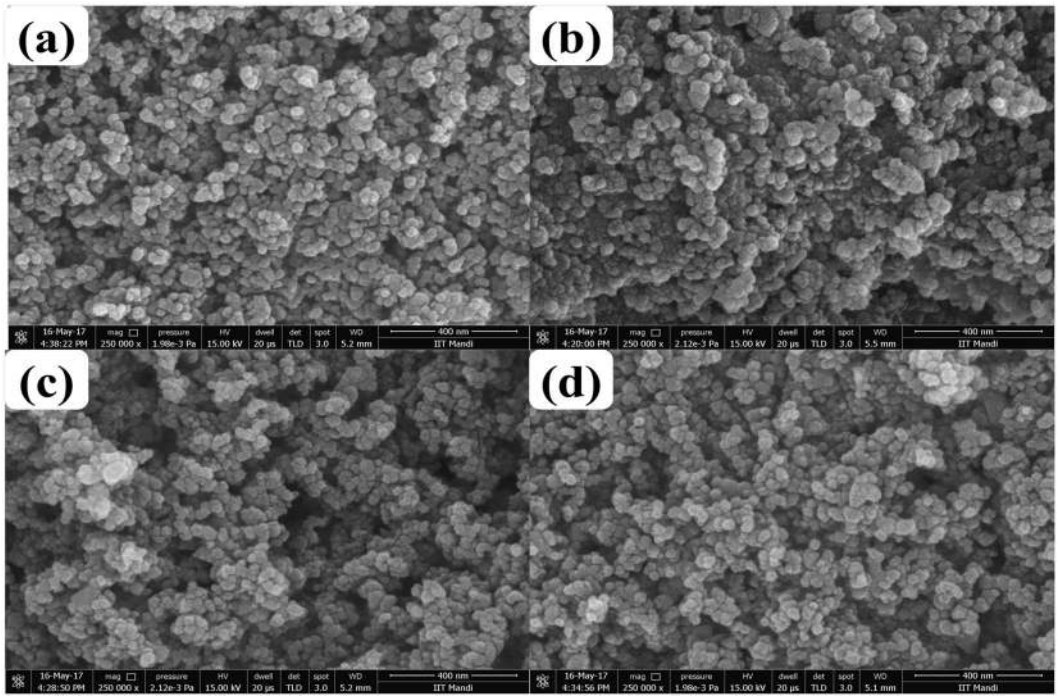


**Figure 4.** SEM images of (**a**) $TiO_2$, (**b**) $TCo_{0.5}N_{1.5}$, (**c**) $TCo_{1.0}N_{1.0}$ and (**d**) $TCo_{1.5}N_{0.5}$.

Moreover, all samples display a narrow size distribution for the primary particles. All SEM results are in good agreement with the XRD data.

*Transmission electron microscopy (TEM).* The TEM was used to observe the morphological and uniformity of structure of the particles. All the doped and codoped particles were small and nearly spherical in shape as shown in Fig. 5. It can be seen that the particle size estimated from the TEM data agrees well with the aforesaid XRD data. Further the incorporation of Co and N with $TiO_2$ in the codoped particles was also confirmed by elemental analysis using energy dispersive X-ray analysis (EDX) (Fig. 6).

*UV-Visible spectra.* Optical properties of Co and N codoped $TiO_2$ were studied using UV–visible spectroscopy by measuring optical spectra in the range of 200–800 nm, in diffuse reflectance mode. Kubelka -Munk (K-M) plot (Fig. 7) was used to assess the band gap energies by extrapolating the linear region of the plot to intersect the photon energy axis; the obtained values are concise in Table 1. For pure $TiO_2$, the band gap value of 3.2 eV was obtained, which is close to the expected value of the anatase phase (3.18 eV). After Co and N codoping, the band gap of $TiO_2$ decreases. On the other hand, substantial narrowing of band gap was perceived after Co and N codoping.

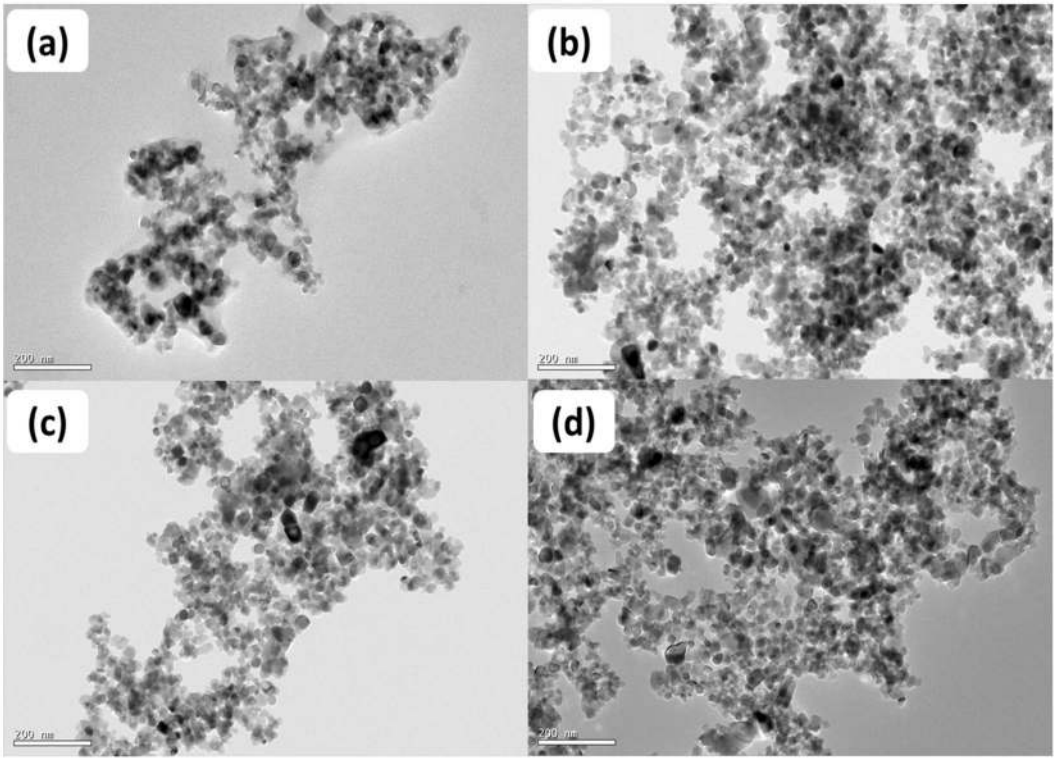


**Figure 5.** TEM images of (**a**) $TiO_2$, (**b**) $TCo_{0.5}N_{1.5}$, (**c**) $TCo_{1.0}N_{1.0}$ and (**d**) $TCo_{1.5}N_{0.5}$.

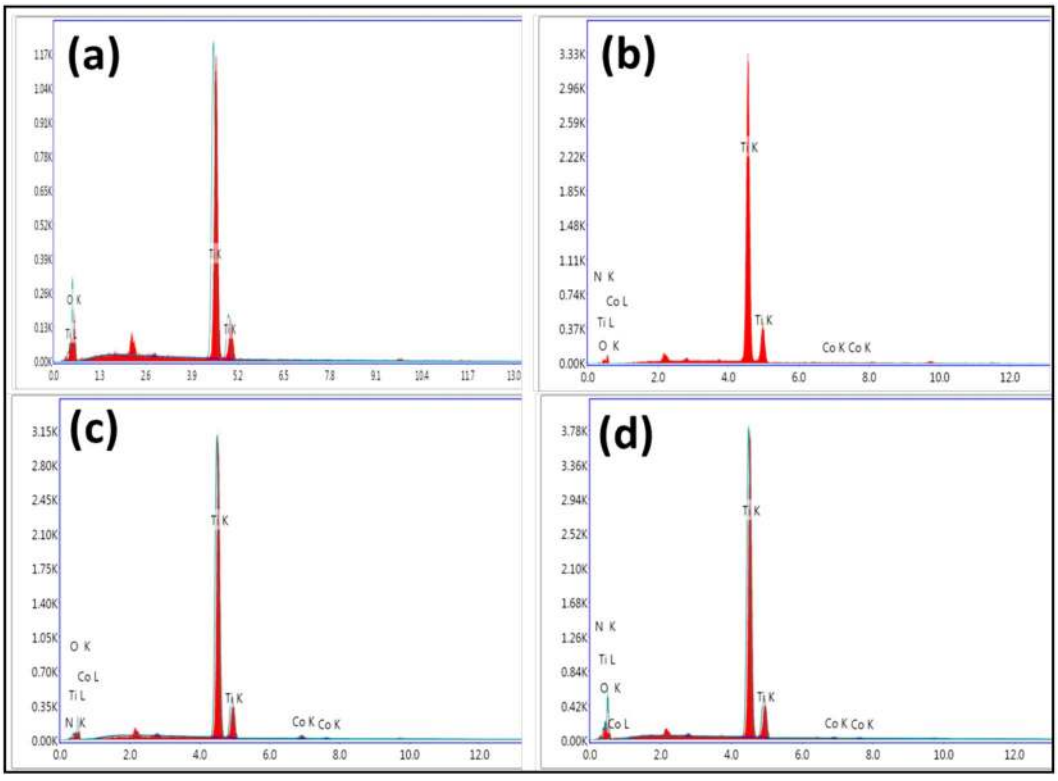


**Figure 6.** EDX mapping of (**a**) $TiO_2$, (**b**) $TCo_{0.5}N_{1.5}$, (**c**) $TCo_{1.0}N_{1.0}$ and (**d**) $TCo_{1.5}N_{0.5}$.

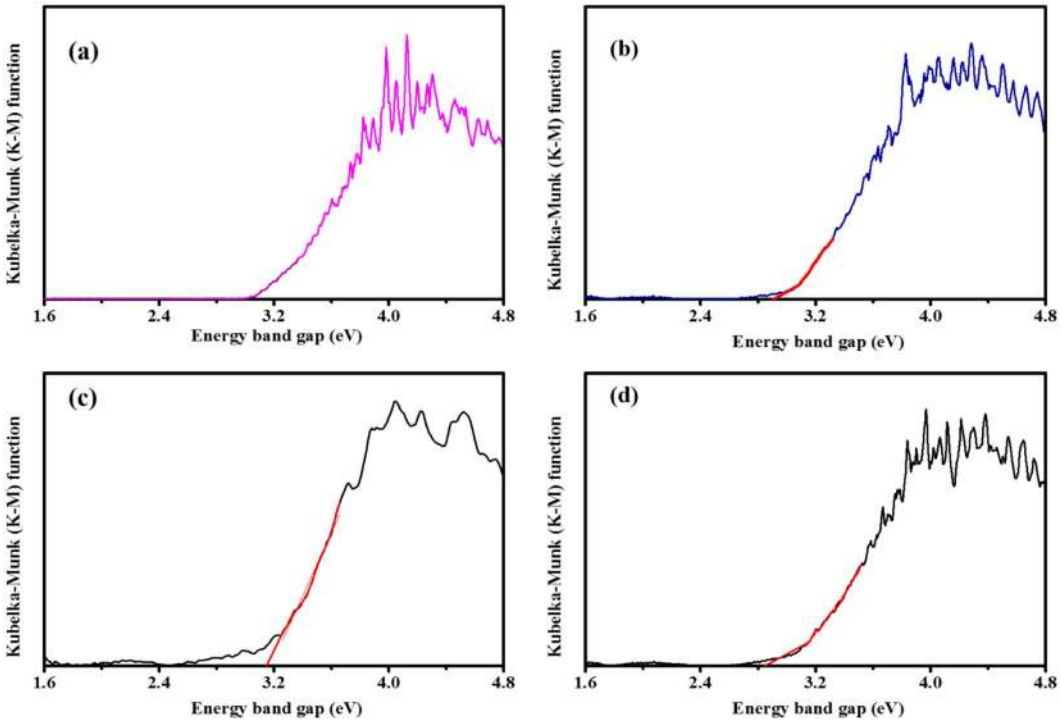


**Figure 7.** Kubelka-Munk (K-M) functionplot (**a**) $TiO_2$, (**b**) $TCo_{0.5}N_{1.5}$, (**c**) $TCo_{1.0}N_{1.0}$ and (**d**) $TCo_{1.5}N_{0.5}$.

*X-ray Photoelectron Spectroscopy (XPS).* X-ray photoelectron spectroscopic analysis was performed on the synthesized catalysts in order to confirm the presence of co-dopants and to decipher the detailed chemical state information of Co, O, N, and Ti and their oxidation states. Figure 8(a) gives the total survey spectrum which indicates the existence of $Ti^{4+}$, $O^{2-}$, $N^{3+}$ and $Co^{2+}$ in the $TCo_{1.0}N_{1.0}$ catalyst prepared. Figure 8(b–f) gives the XPS data for the elements Ti 2p, O 1s, C 1s, Co 2p3, and N1s. The XPS spectrum of other samples (pure $TiO_2$, $TCo_{0.5}N_{1.5}$, $TCo_{1.0}N_{1.0}$, and $TCo_{1.5}N_{0.5}$) were shown in Figs S1–S3.

For the Ti 2 p region (Fig. 8(b)), the peaks of Ti $sp_{3/2}$ and Ti $2p_{1/2}$ at 457.75 eV and 463.45 eV, respectively, they are all in good agreement with the values of $Ti^{4+}$. The similar observations have been reported by Apiwong-ngarm *et al.*[28] (i.e. the peaks of Ti $sp_{3/2}$ and Ti $2p_{1/2}$ at 458.62 eV and 464.36 eV, respectively) and Wang *et al.*[29] (i.e. the peaks of Ti $sp_{3/2}$ and Ti $2p_{1/2}$ at 458.6 eV and 464.3 eV, respectively). No broad FWHM of Ti $2p_{3/2}$ peak signals also indicates the only presence of $Ti^{4+}$ species[29]. The O 1s binding energies (Fig. 8(c)) of all the samples are located at 529 eV, which is assigned to bulk oxide ($O^{2-}$) in the $TiO_2$ lattice. Apiwong-ngarm *et al.*[28] and Zhou *et al.*[30] reported the similar peaks for O 1s. The signals of Co 2p3 (Figure (e)) were found to be weaker than all the others, due to the low doping amount. Co $2p_{3/2}$ peak located at band energies 779.5 eV was ascribed to the presence of $Co_2O_3$ or mixed valent Co2O3 with binding energy 779.4 eV reported in literature[31]. Figure 8(f) shows the XPS spectrum for N 1s. The peak at 399.1 eV demonstrated that nitrogen is incorporated into the $TiO_2$ lattice. This considered to be the evidence of the presence of the Ti–N bond[32].

**Photocatalytic activity.** *Effect of photolysis and adsorption.* To evaluate the effect of photolysis and adsorption on photocatalytic transformation, a series of preliminary experiments were carried out. Photolysis experiments were performed at pH = 5 and concentration of codoped $TiO_2$ 70 mg $l^{-1}$ with an initial concentration of BPA 50 mg $l^{-1}$ for 70 min under solar light. As Fig. 9(a) shows, the photolysis of BPA was 11% only. The present results are in agreement with observation made by Rosenfeldt *et al.*[33], which reported that photolysis of BPA during short time irradiation was insignificant.

On the other hand, adsorption capacity of the catalyst under dark conditions was observed at pH 5 and 50 mg $l^{-1}$ initial concentration of BPA with 70 mg $l^{-1}$ initial concentration of catalyst for 70 min reaction time. The percentage degradation due to adsorption of $TiO_2$, $TCo_{0.5}N_{1.5}$, $TCo_{1.0}N_{1.0}$ and $TCo_{1.5}N_{0.5}$ was 16, 20, 21 and 22% respectively (Fig. 9b).

*Effect of pH.* pH is an important factor in the degradation process. For estimating the optimum pH for the photocatalytic degradation of BPA using codoped $TiO_2$, three different solutions (water containing BPA) have been prepared for which pH were maintained at 3, 5, and 9 respectively. Dose of doped $TiO_2$ catalyst and initial concentration of BPA were 70 mg $l^{-1}$ and 20 mg $l^{-1}$ respectively. It was observed that the degree of disappearance of BPA is quite strong in acidic pH conditions (Fig. 10). The possible explanation of this BPA disappearance at pH = 3 is the amphoteric behavior of semiconducting material and the change of the surface charge properties of $TiO_2$ photocatalyst.

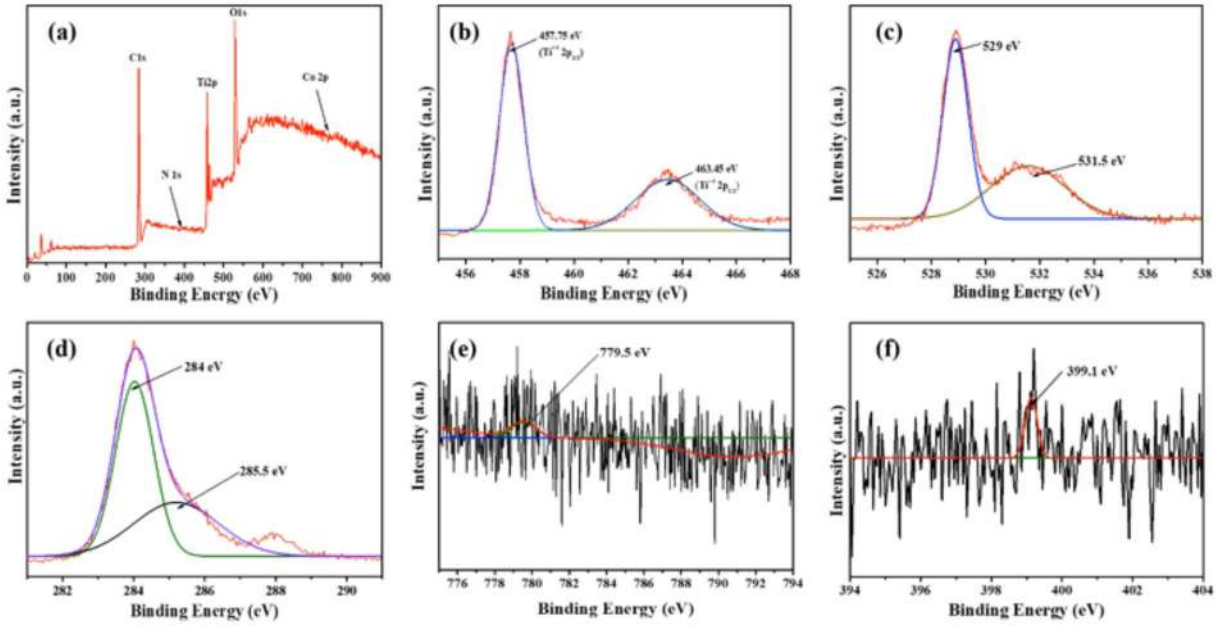


**Figure 8.** XPS of $TCo_{1.0}N_{1.0}$ sample (**a**) whole, (**b**) Ti 2p, (**c**) O 1s, (**d**) C 1s, (**e**) Co 2p3 and (**f**) N 1s.

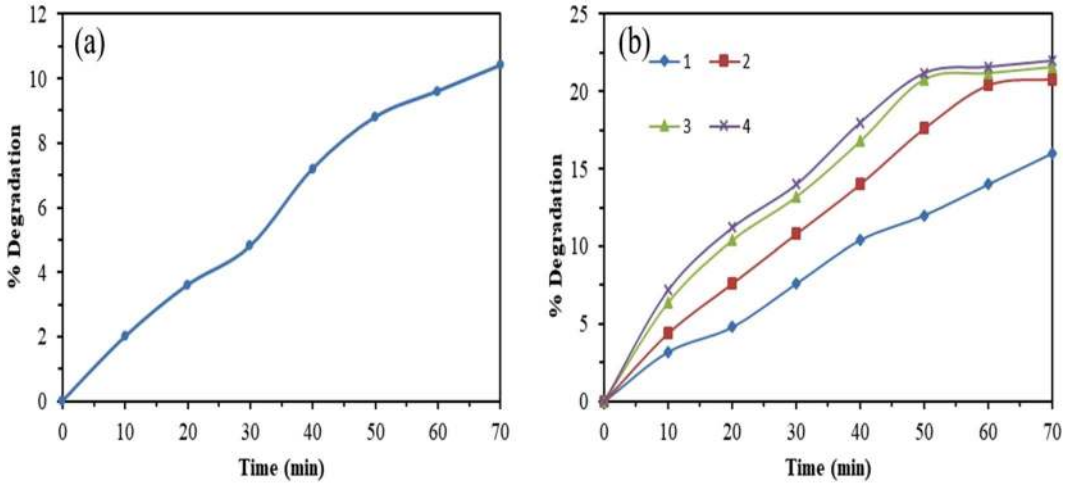


**Figure 9.** (**a**) Photolysis and (**b**) Adsorption of BPA with (1) $TiO_2$, (2) $TCo_{0.5}N_{1.5}$, (3) $TCo_{1.0}N_{1.0}$ and (4) $TCo_{1.5}N_{0.5}$.

*Effect of catalyst dose.* For analyzing the effect of catalyst dose, experiments were performed with different doses of photocatalyst. In above experiments we used 70 mg $l^{-1}$ $TiO_2$ photocatalyst, but herein we have checked 35 mg $l^{-1}$, 105 mg $l^{-1}$, 140 mg $l^{-1}$, and 175 mg $l^{-1}$ $TiO_2$ photocatalyst (Fig. 11) to find the effect of catalyst dose. It is clear from Fig. 11 that the maximum degradation of BPA was observed at the $TiO_2$ concentration of 140 mg $l^{-1}$. Moreover, on further increasing the photocatalyst dose until 175 mg $l^{-1}$, the degradation of BPA decreases. It is due to the greater amount of catalyst, which causes increase in turbidity and thereby it impedes the penetration of light in the reactor, which in turn lowers the photo catalytic efficiency in the given working conditions. Another possible reason for the decrease in rate could be due to the decrease in the portion of the irradiated surface of the catalyst particle due to the obstruction of light in the dense slurry.

*Effect of concentration of BPA.* The effect of the initial concentration of BPA on the degradation of BPA under the solar light was determined. The obtained results have been presented in Fig. 12. The results indicated that the decomposition rate of BPA strongly depends on the initial BPA concentration. The efficiency of photodegradation of BPA decreased with increasing the initial BPA concentration. BPA with 10 mg $l^{-1}$ shows 98% degradation after 140 min. On increasing the concentration of BPA until 50 mg $l^{-1}$ the photodegradation became very slow, presenting a degradation of only 40%. As the initial concentration of BPA increased, more BPA molecules were

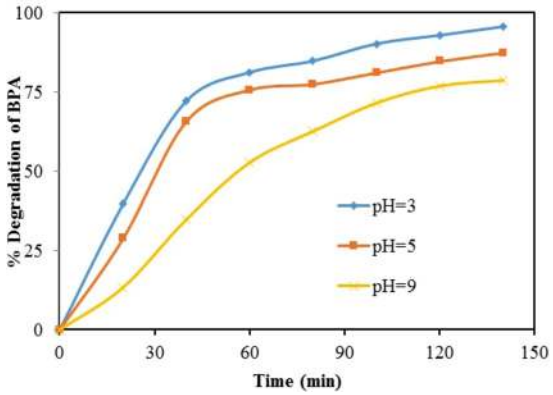


**Figure 10.** Effect of pH on initial rate of degradation of BPA: $[TiO_2]_0 = 70\,mg l^{-1}$, initial concentration of BPA = $20\,mg\,l^{-1}$.

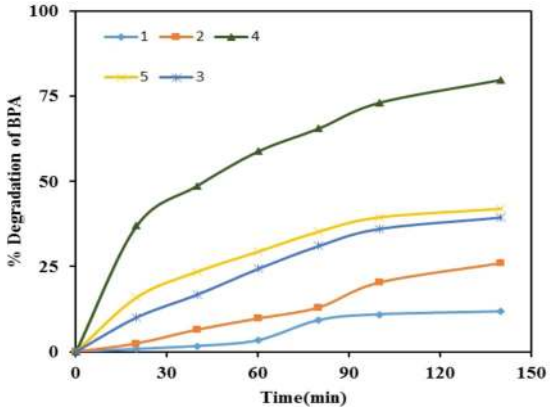


**Figure 11.** Effect of catalyst concentration on initial rate of degradation of BPA: pH = 3, initial concentration of BPA = $20\,mg\,l^{-1}$, $[TiO_2]_0$ = (1) $35\,mg\,l^{-1}$, (2) $70\,mg\,l^{-1}$, (3) $105\,mg\,l^{-1}$, (4) $140\,mg\,l^{-1}$ and (5) $175\,mg\,l^{-1}$.

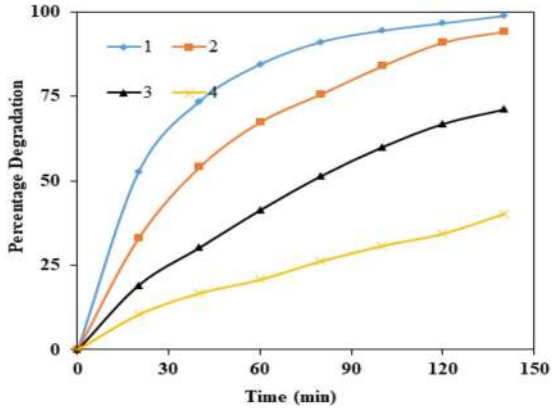


**Figure 12.** Effect of initial concentration of BPA for the degradation of BPA: pH = 3, catalyst concentration = $140\,mg\,l^{-1}$, $[BPA]_0$ = (1) $10\,mg\,l^{-1}$, (2) $30\,mg\,l^{-1}$, (3) $40\,mg\,l^{-1}$, and (4) $50\,mg\,l^{-1}$.

adsorbed on the surface on the catalyst occupying the active sites and therefore the generation of hydroxyl radicals was reduced[34–36]. An increase of the initial BPA concentration results in an increase of the amount of BPA adsorbed on the catalyst surface, affecting the catalytic activity of the photocatalyst[37,38]. Moreover, the reduction of the light path length as the concentration increases could be one of the reasons for decreased catalytic acitivity.

*Effect of dopant content.* Cobalt and nitrogen codoped titania photocatalysts containing different amounts of codoping metal/nonmetal ($TCo_xN_y$, x = 0.5, 1 and 1.5 and y = 1.5, 1.0 and 0.5 respectively) were tested for the

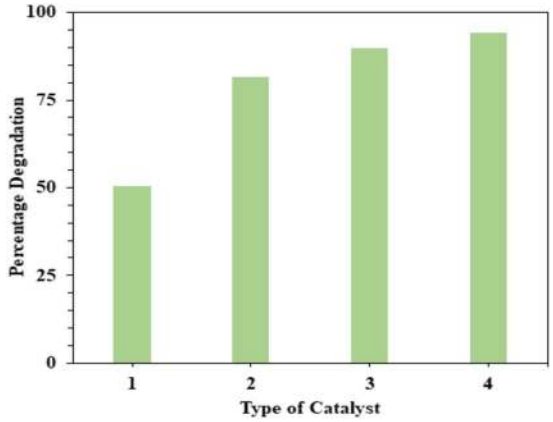


**Figure 13.** Effect of dopant content for the degradation of BPA: pH = 3, catalyst concentration = 140 mg $l^{-1}$, and $[BPA]_o$ = 30 mg $l^{-1}$ (1) $TiO_2$, (2) $TCo_{0.5}N_{1.5}$, (3) $TCo_{1.0}N_{1.0}$ and (4) $TCo_{1.5}$ $N_{0.5}$.

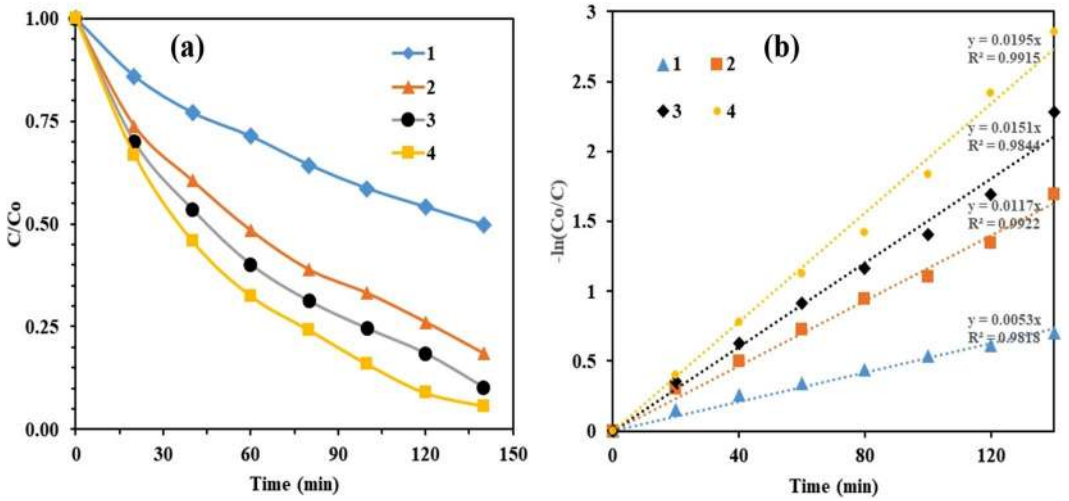


**Figure 14.** (**a**) Degradation and (**b**) reaction kinetics of BPA: pH = 3, catalyst concentration = 140 mg $l^{-1}$, and $[BPA]_o$ = 30 mg $l^{-1}$ (1) $TiO_2$, (2) $TCo_{0.5}N_{1.5}$, (3) $TCo_{1.0}N_{1.0}$ and (4) $TCo_{1.5}$ $N_{0.5}$.

degradation of BPA under solar light UV irradiation. The percentage degradation of BPA vs. cobalt and nitrogen content were presented in Fig. 13. Under analogous conditions, photoactivity was low for pure $TiO_2$ and 0.5% Co content, whereas with 1% of Co codopant in the material lead to an increase in BPA degradation. The photocatalytic degradation of BPA increases for higher (>1%) Co doping levels (Fig. 13). Regarding BPA degradation rates, a maximum degradation rate was observed for 1.5% Co codoping (i.e. $TCo_{1.5}$ $N_{0.5}$).

*Reaction kinetic studies.* A simple power law kinetic model could relate the degradation of BPA. The pseudo first order kinetics in terms of degradation of BPA can be written as:

$$\frac{-d[C]}{dt} = k'[C]$$

where k′ is the pseudo first order rate constant.

Integration (with the limit of $C = C_o$ at $t = 0$) with $C_o$ being the equilibrium concentration of the bulk solution, $\ln(C_o/C) = k't$, where, $C_o$ is the equilibrium concentration of BPA and C is the concentration of BPA at time t.

A plot of $C/C_o$ versus *t* for degradation of BPA has been shown in Fig. 14(a). A linear relationship was observed between degradation rate of BPA and irradiation time (Fig. 14(b)). The kinetic constants are 0.0053, 0.0117, 0.0151, and 0.0195 $min^{-1}$ for $TiO_2$, $TCo_{0.5}N_{1.5}$, $TCo_{1.0}N_{1.0}$, and $TCo_{1.5}$ $N_{0.5}$, respectively. Similar observation has been reported by Sharma *et al.*[2] for the photo-oxidation of BPA with hydrogen peroxide ($H_2O_2$) and sodium persulfate.

In the direction of complete mineralization of BPA and the total degradation during photocatalysis, the total organic carbon (TOC) removal was estimated and has been shown in Fig. 15. The TOC removal showed a good mineralization trend of BPA. In the first 30 minutes of irradiation 52% TOC removal was observed and in the

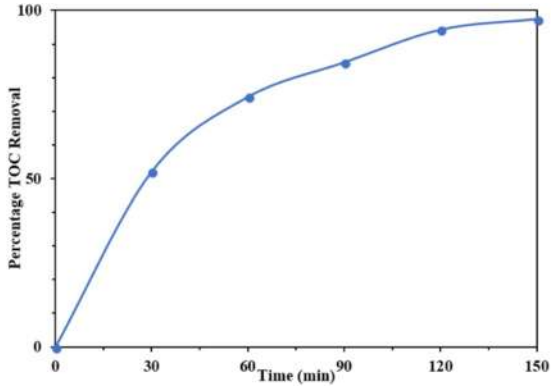


**Figure 15.** TOC removal versus time of BPA: pH = 3, catalyst ($TCo_{1.0}N_{1.0}$) concentration = 140 mg $l^{-1}$, and $[BPA]_o$ = 30 mg $l^{-1}$.

| Retention time (min) (90 min sample) | m/Z | Prominent intermediate compound formed |
|---|---|---|
| 9.9 | 136 | 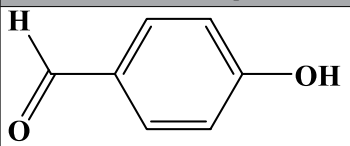 |
| 15.698 | 140 | 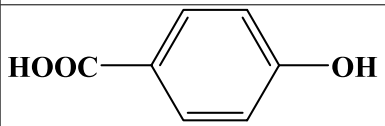 |
| 16.11 | 154 | 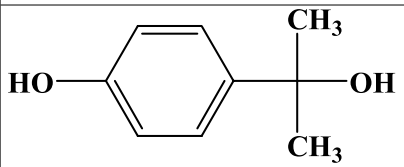 |
| 17.36 | 136 | 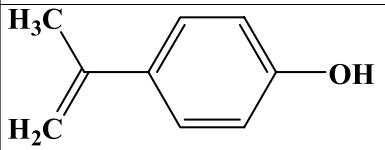 |

**Table 2.** Intermediate compounds recognized from GC-MS analysis of photo-degradation of BPA.

following 140 minutes, 97% TOC removal was observed. It indicates the complete mineralized of BPA at the end of 140 minutes.

*Photodegradation pathway of BPA using codoped $TiO_2$.* The intermediate products formed during the photocatalytic degradation of BPA were identified from the Gas Chromatography – Mass Spectroscopy (GC-MS) analysis as shown in Table 2. Based on the intermediates found during GC-MS analysis, the proposed four possible reaction pathways has been shown in Fig. 16. It was noticed that other chromatographic peaks were also established but could not be positively recognized than the successfully detected compounds, (i.e. the match factor of the spectrum was not significant). It was clear that phenoxyl radicals was produced from all four of initial reactions. These single aromatic intermediates were presumably further oxidized through ring breaking reactions into non-toxic aliphatic acids. Finally, these aliphatic acids were oxidized to carbon dioxide and water.

## Conclusion

Co/N co-doped $TiO_2$ with variable dopant composition have been synthesised by wet impregnation method. Catalysts exhibited changes in properties that could be associated with changes in structure. Dopants like cobalt and nitrogen were observed to disturb the physical properties of the nano particles, producing alterations in crystal structure, energy band gap as well as elemental composition. A decent photocatalytic rate was found by increasing the cobalt composition as a dopant for the degradation of BPA. TOC results revealed the complete mineralization of BPA. GC-MS analysis suggests the possible reaction pathway as well as the intermediates produced during the photocatalytic reaction.

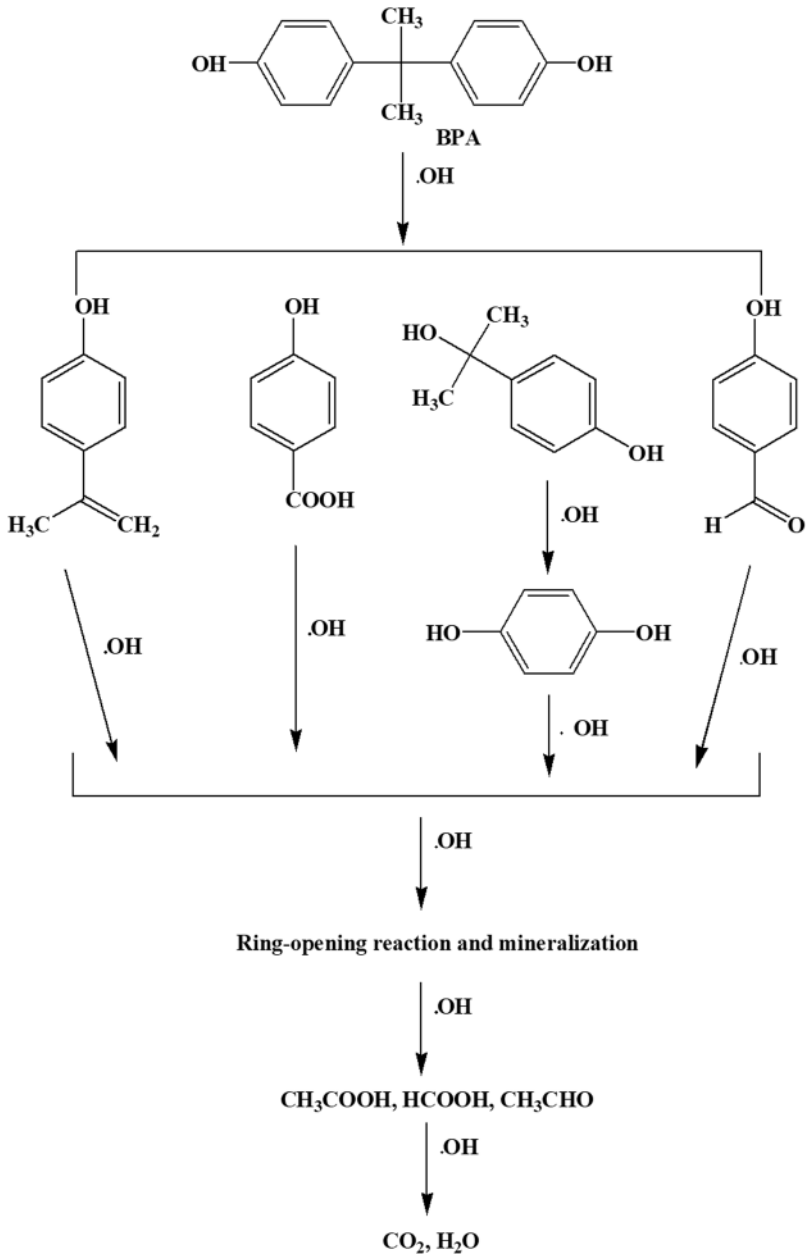


**Figure 16.** Proposed solar photocatalytic degradation reaction pathway of BPA.

## Materials and Methods

**Materials.** Bisphenol-A [2,2-bis (4-hydroxyphenyl) propane or BPA] ($C_{15}H_{16}O_2$) was procured from Sigma Aldrich. Titanium dioxide (Degussa P25) was used as catalyst and obtained from Evonik Degussa Corporation, USA. Cobalt (II) Nitrate Hexahydrate [Co $(NO_3)_2.6H_2O$] and Urea were procured from Sigma Aldrich and were utilized as dopant. Hydrochloric acid (HCL) and sodium hydroxide (NaOH) were purchased from S. D. Fine Chemicals Limited, India and utilized to maintain the pH. For all the tests, distilled water (DW) and methanol were utilized as a solvent.

**Preparation and characterization of codoped $TiO_2$.** The codoped $TiO_2$ nano powder was prepared using the method discussed by Garg *et al.*[23] with a little modification wherein methanol was taken in place of water for suspension of $TiO_2$. 3 gm of Degussa P25 $TiO_2$ has been suspended in 100 ml of methanol, followed by the addition of required amount of Cobalt (II) Nitrate Hexahydrate and urea solution. The obtained slurry was well stirred for 2 h followed by ultrasonication for 10 minutes and kept at rest for 24 hours. The obtained slurry has been thoroughly washed with distilled water for removal of undoped ions before drying in hot air oven at 100 °C for overnight. The solid particles were grounded in agate mortar followed by calcination at 400 °C for 2 hours in muffle furnace. The codoped $TiO_2$ photocatalyst were prepared with codopant concentrations of 2 wt% and were denoted by $TCo_xN_y$ (x = 0.5, 1 and 1.5 and y = 1.5, 1.0 and 0.5 respectively), where x and y are the wt% of Co and N, respectively.

To study the crystal structure and crystallinity of Co-N-$TiO_2$ nanoparticles, X-ray diffraction (XRD) analysis was performed on X'Pert PRO (D8 Advance) XRD diffractometer using Cu K$\alpha$ ($\lambda = 0.15406$ nm) radiation. To investigate the light absorption and optical band gap of the synthesized $TiO_2$ nanoparticles, the UV-vis absorption spectra were obtained with a UV-vis spectrophotometer for determining the binding energy with respect to Co and N. Fourier transform infrared (FTIR) spectra was recorded on Agilent technologies cary 600 series. Transmission Electron Microscope (TEM) characterization was done by using an FEI TECNAI G2 20 - TWIN 120 kV and Scanning Electron Microscope (SEM) characterization was done by using an FEI-Nova nano SEM-450. Energy-dispersive X-ray spectroscopy (EDX) attached to the SEM was used to determine the composition of elements. Surface composition and electronic structures were analyzed by X-ray photoelectron spectroscopy using an ULVAC-PHI (model: PHI5000VersaProbeII) XPS system.

**Photocatalytic degradation of Bisphenol-A (BPA).** The photocatalytic activity of codoped photocatalysts were examined for the degradation BPA under solar light followed by adsorption-desorption equilibrium in dark for 20 mins. During the solar light irradiation experiments, stirring was maintained by magnetic stirrer to manage the solution homogeneous. A fixed amount of sample was withdrawn at different time intervals over 140 min and placed into different syringes and filters. The BPA concentration was determined using a UV-vis spectrophotometer (Perkin Elmer Lambda 35UV-Vis spectrophotometer) at $\lambda_{max} = 277$ nm followed by centrifugation for the separation of catalyst. The percentage photodegradation of BPA was calculated using the equation (4):

$$\text{Percentage photodegradation of BPA} = \frac{C_o - C}{C_o} \times 100 \quad (4)$$

Where, $C_o$ is the initial concentration of BPA and C is the concentration of BPA at time 't'.

For complete mineralization of the BPA solution, the total organic carbon (TOC) content was estimated using Schimadzu model TOC-$V_{CPH}$ Total Organic Carbon Analyzer.

Gas chromatography- mass spectroscopy (GC-MS) of the photo-degraded BPA wastewater was carried out to identify the various intermediates produced during photocatalytic degradation of BPA in wastewater. The GC-MS analysis was carried out by Perkin Elmer Clarus 500 GC coupled with a Perkin Elmer Clarus 500 mass spectrometer.

## References


1. Esplugas, S., Bila, D. M., Krause, L. G. T. & Dezotti, M. Ozonation and advanced oxidation technologies to remove endocrine disrupting chemicals (EDCs) and pharmaceuticals and personal care products (PPCPs) in water effluents. *Journal of Hazardous Materials* **149**, 631–642, https://doi.org/10.1016/j.jhazmat.2007.07.073 (2007).
2. Sharma, J., Mishra, I. M. & Kumar, V. Mechanistic study of photo-oxidation of bisphenol-A (BPA) with hydrogen peroxide ($H_2O_2$) and sodium persulfate (SPS). *Journal of Environmental Management* **166**, 12–22, https://doi.org/10.1016/j.jenvman.2015.09.043 (2016).
3. Garg, A., Sangal, V. K. & Bajpai, P. K. Decolorization and degradation of Reactive Black 5 dye by photocatalysis: Modeling, optimization and kinetic study. *Desalination and Water Treatment* **57**, 18003–18015, https://doi.org/10.1080/19443994.2015.1086697 (2016).
4. Fujishima, A., Zhang, X. & Tryk, D. A. $TiO_2$ photocatalysis and related surface phenomena. *Surface Science Reports* **63**, 515–582, https://doi.org/10.1016/j.surfrep.2008.10.001 (2008).
5. Wilke, K. & Breuer, H. D. The influence of transition metal doping on the physical and photocatalytic properties of titania. *Journal of Photochemistry and Photobiology A: Chemistry* **121**, 49–53, https://doi.org/10.1016/S1010-6030(98)00452-3 (1999).
6. Agrios, A. G. & Pichat, P. State of the art and perspectives on materials and applications of photocatalysis over $TiO_2$. *Journal of Applied Electrochemistry* **35**, 655–663, https://doi.org/10.1007/s10800-005-1627-6 (2005).
7. Gaya, U. I. & Abdullah, A. H. Heterogeneous photocatalytic degradation of organic contaminants over titanium dioxide: A review of fundamentals, progress and problems. *Journal of Photochemistry and Photobiology C: Photochemistry Reviews* **9**, 1–12, https://doi.org/10.1016/j.jphotochemrev.2007.12.003 (2008).
8. Carp, O., Huisman, C. L. & Reller, A. Photoinduced reactivity of titanium dioxide. *Progress in Solid State Chemistry* **32**, 33–177, https://doi.org/10.1016/j.progsolidstchem.2004.08.001 (2004).
9. Asahi, R., Morikawa, T., Ohwaki, T., Aoki, K. & Taga, Y. Visible-light photocatalysis in nitrogen-doped titanium oxides. *Science* **293**, 269–271, https://doi.org/10.1126/science.1061051 (2001).
10. Yu, J. C., Jiaguo, W. Z. & Lizhi Effects of $F^-$ doping on the photocatalytic activity and microstructures of nanocrystalline $TiO_2$ powders. *Chemistry of Materials* **14**, 3808–3816, https://doi.org/10.1021/cm020027c (2002).
11. Sakthivel, S. & Kisch, H. Daylight photocatalysis by carbon-modified titanium dioxide. *Angewandte Chemie International Edition* **42**, 4908–4911, https://doi.org/10.1002/anie.200351577 (2003).
12. Diwald, O., Thompson, T. L., Goralski, E. G., Walck, S. D. & Yates, J. T. The effect of nitrogen ion implantation on the photoactivity of $TiO_2$ rutile single crystals. *The Journal of Physical Chemistry B* **108**, 52–57, https://doi.org/10.1021/jp030529t (2004).
13. Park, J. H., Kim, S. & Bard, A. J. Novel carbon-doped $TiO_2$ nanotube arrays with high aspect ratios for efficient solar water splitting. *Nano Letters* **6**, 24–28, https://doi.org/10.1021/nl051807y (2006).
14. Dong, L. *et al*. Enhanced photocatalytic degradation properties of nitrogen-doped titania nanotube arrays. *Transactions of Nonferrous Metals Society of China* **19**, 1583–1587, https://doi.org/10.1016/S1003-6326(09)60074-1 (2009).
15. Ao, Y., Xu, J., Zhang, S. & Fu, D. A one-pot method to prepare N-doped titania hollow spheres with high photocatalytic activity under visible light. *Applied Surface Science* **256**, 2754–2758, https://doi.org/10.1016/j.apsusc.2009.11.023 (2010).
16. Pelaez, M. *et al*. A review on the visible light active titanium dioxide photocatalysts for environmental applications. *Applied Catalysis B: Environmental* **125**, 331–349, https://doi.org/10.1016/j.apcatb.2012.05.036 (2012).
17. Wu, J. C. S. & Chen, C.-H. A visible-light response vanadium-doped titania nanocatalyst by sol–gel method. *Journal of Photochemistry and Photobiology A: Chemistry* **163**, 509–515, https://doi.org/10.1016/j.jphotochem.2004.02.007 (2004).
18. Gupta, S. M. & Tripathi, M. A review of $TiO_2$ nanoparticles. *Chinese Science Bulletin* **56**, 1639–1657, https://doi.org/10.1007/s11434-011-4476-1 (2011).
19. Klosek, S. & Raftery, D. Visible Light Driven V-Doped $TiO_2$ Photocatalyst and Its Photooxidation of Ethanol. *The Journal of Physical Chemistry B* **105**, 2815–2819, https://doi.org/10.1021/jp004295e (2001).

20. Ghasemi, S., Rahimnejad, S., Setayesh, S. R., Rohani, S. & Gholami, M. R. Transition metal ions effect on the properties and photocatalytic activity of nanocrystalline $TiO_2$ prepared in an ionic liquid. *Journal of Hazardous Materials* **172**, 1573–1578, https://doi.org/10.1016/j.jhazmat.2009.08.029 (2009).
21. Gupta, N. & Pal, B. Photocatalytic activity of transition metal and metal ions impregnated $TiO_2$ nanostructures for iodide oxidation to iodine formation. *Journal of Molecular Catalysis A: Chemical* **371**, 48–55, https://doi.org/10.1016/j.molcata.2013.01.020 (2013).
22. Subramanian, M., Vijayalakshmi, S., Venkataraj, S. & Jayavel, R. Effect of cobalt doping on the structural and optical properties of $TiO_2$ films prepared by sol–gel process. *Thin Solid Films* **516**, 3776–3782, https://doi.org/10.1016/j.tsf.2007.06.125 (2008).
23. Garg, A., Singh, A., Sangal, V. K., Bajpai, P. K. & Garg, N. Synthesis, characterization and anticancer activities of metal ions Fe and Cu doped and co-doped $TiO_2$. *New Journal of Chemistry* **41**, 9931–9937, https://doi.org/10.1039/C7NJ02098H (2017).
24. Chen, X. & Mao, S. S. Titanium dioxide nanomaterials: Synthesis, properties, modifications, and applications. *Chemical Reviews* **107**, 2891–2959, https://doi.org/10.1021/cr0500535 (2007).
25. Zhang, Y., Harris, C. X., Wallenmeyer, P., Murowchick, J. & Chen, X. Asymmetric lattice vibrational characteristics of rutile $TiO_2$ as revealed by laser power dependent raman spectroscopy. *The Journal of Physical Chemistry C* **117**, 24015–24022, https://doi.org/10.1021/jp406948e (2013).
26. Hamal, D. B. & Klabunde, K. J. Synthesis, characterization, and visible light activity of new nanoparticle photocatalysts based on silver, carbon, and sulfur-doped $TiO_2$. *Journal of Colloid and Interface Science* **311**, 514–522, https://doi.org/10.1016/j.jcis.2007.03.001 (2007).
27. Wu, M. *et al.* Efficient one-pot synthesis of Ag nanoparticles loaded on N-doped multiphase $TiO_2$ hollow nanorod arrays with enhanced photocatalytic activity. *Applied Surface Science* **256**, 7125–7130, https://doi.org/10.1016/j.apsusc.2010.05.038 (2010).
28. Apiwong-ngarm, K. *et al.* Photocatalytic activities of Fe–Cu/$TiO_2$ on the mineralization of oxalic acid and formic acid under visible light irradiation. *Powder Technology* **266**, 447–455, https://doi.org/10.1016/j.powtec.2014.06.061 (2014).
29. Wang, Q., Xu, S. & Shen, F. Preparation and characterization of $TiO_2$ photocatalysts co-doped with iron (III) and lanthanum for the degradation of organic pollutants. *Applied Surface Science* **257**, 7671–7677, https://doi.org/10.1016/j.apsusc.2011.03.157 (2011).
30. Wenfang, Z., Qingju, L., Zhongqi, Z. & Ji, Z. Preparation and properties of vanadium-doped $TiO_2$ photocatalysts. *Journal of Physics D: Applied Physics* **43**, 035301–035306 (2010).
31. Chekuri, R. D. & Tirukkovalluri, S. R. Synthesis of cobalt doped titania nano material assisted by gemini surfactant: Characterization and application in degradation of Acid Red under visible light irradiation. *South African Journal of Chemical Engineering* **24**, 183–195, https://doi.org/10.1016/j.sajce.2017.10.001 (2017).
32. Batalović, K. *et al.* Modification of N-doped $TiO_2$ photocatalysts using noble metals (Pt, Pd) – a combined XPS and DFT study. *Physical Chemistry Chemical Physics* **19**, 7062–7071, https://doi.org/10.1039/C7CP00188F (2017).
33. Rosenfeldt, E. J. & Linden, K. G. Degradation of endocrine disrupting chemicals bisphenol A, ethinyl estradiol, and estradiol during UV photolysis and advanced oxidation processes. *Environmental Science & Technology* **38**, 5476–5483, https://doi.org/10.1021/es035413p (2004).
34. Alaton, I. A. & Balcioglu, I. A. Photochemical and heterogeneous photocatalytic degradation of waste vinylsulphone dyes: a case study with hydrolyzed Reactive Black 5. *Journal of Photochemistry and Photobiology A: Chemistry* **141**, 247–254, https://doi.org/10.1016/S1010-6030(01)00440-3 (2001).
35. Daneshvar, N., Salari, D. & Khataee, A. R. Photocatalytic degradation of azo dye Acid Red 14 in water: investigation of the effect of operational parameters. *Journal of Photochemistry and Photobiology A: Chemistry* **157**, 111–116, https://doi.org/10.1016/S1010-6030(03)00015-7 (2003).
36. Grzechulska, J. & Morawski, A. W. Photocatalytic decomposition of azo-dye Acid Black 1 in water over modified titanium dioxide. *Applied Catalysis B: Environmental* **36**, 45–51, https://doi.org/10.1016/S0926-3373(01)00275-2 (2002).
37. Cater, S. R., Stefan, M. I., Bolton, J. R. & Safarzadeh-Amiri, A. UV/$H_2O_2$ treatment of methyl tert-butyl ether in contaminated waters. *Environmental Science & Technology* **34**, 659–662, https://doi.org/10.1021/es9905750 (2000).
38. Malato, S., Blanco, J., Richter, C., Braun, B. & Maldonado, M. I. Enhancement of the rate of solar photocatalytic mineralization of organic pollutants by inorganic oxidizing species. *Applied Catalysis B: Environmental* **17**, 347–356, https://doi.org/10.1016/S0926-3373(98)00019-8 (1998).


## Acknowledgements

Advanced Materials Research Center (AMRC) and BioX centre at IIT Mandi are gratefully acknowledged for providing facilities to carry this work. Financial assistance from UGC (JRF) for Mr. Ashutosh Singh and Ramanujan Fellowship SERB fellowship to Dr. Neha Garg (SB/S2/RJN-072/2015) is highly acknowledged.

## Author Contributions

A.G. designed, performed, analyzed most of the experiments and wrote the manuscript. T.S. worked with A.G. (as a student) for performing the experiments. A.S., S.S. worked with N.G. (as students) for performing the experiments. S.S. worked with A.G. (as a student) for performing the experiments related to HPLC/GC-MS and TOC. A.N. worked with S.R.Y. (as a student) for performing the experiments related to XPS. S.R.Y. designed and analyzed XPS experiments. V.K.S. analyzed HPLC/GC-MS data. N.G. designed, analyzed the experiments and supervised the study.

## Additional Information

**Supplementary information** accompanies this paper at https://doi.org/10.1038/s41598-018-38358-w.

**Competing Interests:** The authors declare no competing interests.

**Publisher's note:** Springer Nature remains neutral with regard to jurisdictional claims in published maps and institutional affiliations.

**Open Access** This article is licensed under a Creative Commons Attribution 4.0 International License, which permits use, sharing, adaptation, distribution and reproduction in any medium or format, as long as you give appropriate credit to the original author(s) and the source, provide a link to the Creative Commons license, and indicate if changes were made. The images or other third party material in this article are included in the article's Creative Commons license, unless indicated otherwise in a credit line to the material. If material is not included in the article's Creative Commons license and your intended use is not permitted by statutory regulation or exceeds the permitted use, you will need to obtain permission directly from the copyright holder. To view a copy of this license, visit http://creativecommons.org/licenses/by/4.0/.

© The Author(s) 2019